

Submitted to Optics Letters, December 1991

**Cu:SILICA NANOCUSTER COMPOSITE MATERIAL WITH
PICOSECOND THIRD-ORDER NONLINEAR OPTICAL RESPONSE**

R. F. HAGLUND, Jr.^(1,3), L. YANG,^(1,3) R. H. MAGRUDER, III⁽²⁾,
K. BECKER,⁽³⁾ J. E. WITTIG⁽²⁾ and R. A. ZUHR⁽⁴⁾

Departments of ⁽¹⁾Physics and Astronomy and of ⁽²⁾Materials Science and Engineering
and ⁽³⁾Free-Electron Laser Center for Biomedical and Materials Research

Vanderbilt University, Nashville, TN 37235

⁽⁴⁾Solid-State Division, Oak Ridge National Laboratory, Oak Ridge, TN 37831

ABSTRACT

We report the creation of a novel composite nonlinear optical material by implanting Cu ions in fused silica. The implanted Cu ions aggregate at room temperature to form nm-size polycrystalline clusters in a high-density thin (~ 150 nm) layer just beneath the surface of the substrate. Measurements of the Kerr-type third-order nonlinear susceptibility $\chi^{(3)}$ of this material shows that it has a response time no longer than 6 ps and a magnitude of order 10^{-8} esu. The nonlinearity is enhanced for laser wavelengths near the surface plasmon resonance of the copper colloids.

The development of practical optical computing and communication devices will require materials with large $\chi^{(3)}$ fabricated by techniques compatible with microelectronics processing technology. Metallic nanoclusters embedded in a dielectric are potentially attractive for these applications, since they exhibit a *nonresonant* ultrafast nonlinear response at the bulk or surface plasmon frequency of the metal. The response time of gold colloids in water has been shown to be less than 5 psec,¹ and the size of $\chi^{(3)}$ and response time of gold colloids both in water² and in Schott (RG6) filter glass³ has been found to depend on colloid shape and size distributions. Enhancements in $\chi^{(3)}$ of several orders of magnitude have been predicted for clusters embedded in dielectrics.⁴ However, metallic colloids have not previously been fabricated in a form compatible with microelectronics technology.

In this paper, we report what to our knowledge is the first observation of picosecond optical nonlinearity in copper clusters produced by ion implantation in silicon dioxide. The Cu clusters have diameters in the 2-28 nm range, as shown by transmission electron microscopy, and are implanted in 150-nm-thick layers. Electron diffraction measurements show that the clusters are polycrystalline, face-centered-cubic structures; the smallest of them could be expected to exhibit quantum size effects. The observed electronic nonlinearity is of the Kerr type, and has a response time no longer than 5.5 ps pulses. The nonlinear index is strongly enhanced at wavelengths near the peak of the surface plasmon resonance in the copper nanoclusters, and has a magnitude of order $10^{-10} \text{ cm}^2 \cdot \text{W}^{-1}$, comparable to the values observed for semiconductor microcrystallites such as $\text{Cd}_x\text{S}_{1-x}$.

Our sample for this experiment was made by implanting a high purity fused silica (Spectrosil®) disk 20 mm in diameter and 1 mm thick with Cu^+ ions at 160 keV energy at room temperature to a total dose of $12 \cdot 10^{16} \text{ ions} \cdot \text{cm}^{-2}$. The ion beam was electrostatically rastered to provide uniform implantation, and the current density was $2.5 \mu\text{A} \cdot \text{cm}^{-2}$, holding the macroscopic

temperature of the substrate below 50 °C. The Cu concentration and depth profiles of the implanted ions were determined by He⁺ ion backscattering (RBS). The total ion dose calculated from RBS was typically 90% of the integrated current measured during implantation, indicating minimal sample charging. The RBS spectra of the implanted layers are bimodal: the larger peak is about twice the size of the smaller and appears nearer the surface. The implanted layer was some 150 nm thick FWHM.

Samples for TEM analysis were prepared by standard grinding, ion-milling and back-thinning techniques, and examined in a Philips CM20/T scanning transmission electron microscope operating at 200 kV. As shown in the bright-field image in Figure 1, the sample clearly contains spherical particles embedded in the silica matrix. This view does not reveal the depth distribution of the nanoclusters; cross-sectional TEM measurements indicate that the larger particles are located closer to the surface in the region of the primary peak in the RBS spectrum; the smaller clusters are beneath this highest-dose region.⁵ Measurements made while tilting the sample revealed that these colloids are spherical in shape with random crystallographic orientation. Electron diffraction measurements, shown in the insert to Fig. 1, display a ring pattern characteristic of face centered cubic (FCC) polycrystalline metallic copper, superimposed on the diffuse diffracted intensity from the amorphous silica matrix.

Particle size distributions were obtained from projected diameters of the clusters from the TEM bright-field images. Regions of the TEM samples were selected which had adequate thickness to represent the overall particle size distribution. By assuming a spherical geometry and a foil thickness equal to the FWHM depth calculated from the RBS profile, these particle-size measurements were used to calculate the areal and volumetric densities listed in Table 1. The computed areal density was in close agreement with that from the RBS measured values. Elsewhere we have reported that such parameters of the nanoclusters as average cluster size, size

distribution and volume fraction are affected and can be controlled both by total dose per side and dose rate.⁶ The distribution of sizes is roughly uniform from 5 nm to 25 nm diameter; the total number of clusters is estimated to be $5.1 \cdot 10^4 \mu\text{m}^{-3}$ in the implanted layer. For purposes of comparison, a 5-nm-diameter fcc copper sphere contains some 1800 atoms. For clusters with diameters below 10 nm, quantum size effects are expected.⁷

TABLE I: Characteristics of Implanted Sample

Sample	Nominal Dose (ions·cm ⁻²)	Number of Sides Implanted	RBS Dose (ions·cm ⁻²)	Current Density (μA·cm ⁻²)	Areal Density (ions·cm ⁻²)	Volume Fraction (%)
1	$12 \cdot 10^{16}$	1	$10 \cdot 10^{16}$	2.5	$9.5 \cdot 10^{16}$	7.5

Differential optical absorption measurements on the Cu:silica sample were made over the wavelength range from 650 to 200 nm (1.8 to 6.2 eV) using a Cary 14 dual beam spectrophotometer interfaced to a microcomputer with an unimplanted sample in the reference beam. Absorption measurements were made at three different positions on the sample; scatter in the data from these three points was less than $\pm 5\%$. The absorption spectrum exhibits a peak at 2.2 eV (the solid curve in Fig. 2) which can be attributed to the Cu surface plasmon resonance. The ratio of plasmon peak to background is preparation dependent.⁸ A significant rise (and in some cases, a peak) in absorption near 5 eV is due to ion-beam-induced radiation damage, in particular the formation of the E' and B₂ electronic defects; there is also probably a contribution from plasmon formation.⁹

The nonlinear index of refraction n_2 is defined in terms of the ordinary linear index n_0 and the (complex) third-order nonlinear dielectric susceptibility $\chi^{(3)}$ by:

$$n = n_0 + \gamma \cdot I, \quad \gamma = \frac{4\pi}{3n_0} 10^{-8} \cdot \text{Re}[\chi^{(3)}] \quad (1)$$

where n_0 is the linear index of refraction and I is the laser intensity. The nonlinear index of refraction was measured with the Z-scan method in an optical set-up described by Becker *et al.*¹⁰

The light source was a 5.5 ps, cavity-dumped tunable dye laser with a 3.8 MHz pulse repetition rate and 100 mW average power. Peak irradiance of the dye laser near the top of its tuning curve is $\sim 2 \cdot 10^9$ W·cm⁻². A 1-mm thick sample of CS₂ was used as a reference for calibrating the Z-scan and our sample. The laser intensity in the Cu-implanted layer was varied by translating the sample through the focal plane of a 150-mm lens on a computer-controlled translation stage. The sample acts as a second lens in series, having an intensity-dependent focal length. The transmitted laser intensity was monitored by a power meter located behind a beam-limiting aperture 90 cm from the focal plane, normalized to the signal from a beamsplitter placed before the focusing lens. For a material with a positive nonlinear index of refraction, moving the sample toward, and then away, from the focal plane causes an initial decrease in the normalized far-field intensity, followed by a recovery to unity at the focal plane and a subsequent increase in intensity.

Typical Z-scan plots for our picosecond measurements have been shown elsewhere.⁶ The analysis we use is based on paraxial optical ray-tracing for the equivalent two-lens system, and is described in detail in a forthcoming publication.¹¹ For a thin, highly absorbing layer embedded in a transparent dielectric, the intensity-dependent part of the refractive index $\gamma = \Delta n/I$ is

$$\gamma = \frac{I_{\max} - I_{\min}}{I_{\max} + I_{\min}} \cdot \frac{n_0 r_0^2}{z_0 I_0 L}, \quad z_0 \equiv \frac{\pi r_0^2}{\lambda} \quad (2)$$

where I_{\max} and I_{\min} are the maximum and minimum intensities recorded in the Z-scan; I_0 is the laser peak intensity at the focal spot, r_0 is the radius of the Gaussian beam profile at the focal plane, L is the thickness of the implanted layer, and z_0 is the diffraction length.

Figure 2 shows the results of Z-scan measurements at several wavelengths between 570 and 600 nm - near the 2.2 eV absorption peak in the spectrum of the samples. The data are values of $\text{Re}[\chi^{(3)}]$ which were extracted from the Z-scan measurements of γ , and are of order of 10^{-8} esu. The fact that $\chi^{(3)}$ exhibits a maximum around 570 nm supports the idea that excitation of the surface plasmon resonance is responsible for the third-order nonlinearity. These values for the nonlinear index are much smaller than the thermo-optic nonlinear susceptibility of $\chi^{(3)} \sim 10^{-6}$ esu reported earlier for 100 ps FWHM laser pulses at 532 nm.¹² This is because at 5.5 ps pulse length, only fast electronic effects of the Kerr type contribute to $\chi^{(3)}$, while at 100 ps pulse length, the high absorption of the sample ($\alpha \sim 10^4 \text{ cm}^{-1}$) leads to thermal self focusing.

Both the magnitude and the enhancement of $\chi^{(3)}$ in Cu:silica resemble the measurements of $\text{Im}[\chi^{(3)}]$ previously carried out on gold colloids in ruby-gold glass and in aqueous solution. The major contribution to this electronic Kerr-type nonlinearity in Au has been shown to arise from photoexcitation of electrons in the conduction band owing to the weak specific heat and consequent ease of raising these electrons to temperatures of many hundreds of degrees.¹ Transient thermorefectance spectroscopy on a 400-nm-thick evaporated Cu film shows that this same hot-electron contribution should be effective in Cu clusters, because several electron-lattice collisions are required to thermalize the incident photon energy in that material also.¹³ In addition, following the analogy with the Au clusters, we expect an *interband* contribution to the nonlinear susceptibility arising from the photoexcitation of electrons from the *d*-band near the *X* point of the Brillouin zone to the *p*-conduction-band states near the Fermi energy. The magnitude of this contribution to $\chi^{(3)}$ in gold is largely imaginary and of order $2 \cdot 10^{-8}$ esu - close to the values of $\text{Re}[\chi^{(3)}]$ measured in our present experiment. It is anticipated that there should be no quantum size effect observed for the broad distribution of relatively large nanoclusters in our sample, since those effects are likely to be seen only for clusters smaller than 2-3 nm in diameter.

The exact relationships between $\chi^{(3)}$ or γ and such materials-preparation parameters as total implantation dose, current density and temperature are currently under investigation. It appears that these parameters determine both the cluster size and cluster size distribution. By controlling the cluster properties, it may be possible to tailor the optical properties for specific applications in optical waveguides and other devices, as well as to enhance the nonlinear optical response. The possibility of controlling the characteristics of nanoclusters through the ion implantation process is particularly intriguing in light of predictions of large enhancements in the third-order nonlinearity for metal-dielectric composite structures created in a nonlinear host matrix.³

In summary, we have shown that it is possible to embed metallic Cu clusters in fused silica using ion-implantation procedures compatible with microelectronics processing techniques to create a novel nonlinear composite material. The ion implanted layers exhibit an electronic nonlinear susceptibility $\chi^{(3)}$ of the Kerr type; the measured nonlinear refractive index is $\gamma \sim 10^{-10} \text{ cm}^2 \cdot \text{W}^{-1}$, comparable to values for II-VI semiconductor nanocrystallites.¹⁴ As we have shown elsewhere, the mean size and size distribution of the clusters can be controlled by varying ion implantation parameters. Thus, using the ion-implantation technique, it should be possible to fabricate metallic nanoclusters in a variety of interesting geometries and at a volumetric density compatible with silica-based optoelectronic device technology.

Acknowledgements

Research at Vanderbilt University was supported in part by the Army Research Office under contract DAAL03-91G-0028 and by the Office of Naval Research through the Free-Electron Laser program for Biomedical and Materials Research. Oak Ridge National Laboratory is partially supported by the Division of Materials Science, U. S. Department of Energy, under contract DE-AC05-84OR21400 with Martin-Marietta Energy Systems, Inc.

REFERENCES

1. F. Hache, D. Ricard, C. Flytzanis and U. Kreibig, *Appl. Phys. A* **47**, 347 (1988).
2. M. J. Bloemer, J. W. Haus and P. R. Ashley, *J. Opt. Soc. Am. B* **7**, 790 (1990).
3. J. W. Haus, N. Kalyaniwalla, R. Inguva, M. Bloemer and C. M. Bowden, *J. Opt. Soc. Am. B* **6**, 797 (1989).
4. J. W. Haus, R. Inguva and C. M. Bowden, *Phys. Rev. A* **40**, 5729 (1989).
5. H. Hosono, private communication and *J. Non-Cryst. Solids*, to be published.
6. R. H. Magruder III, R. F. Haglund, Jr., L. Yang, K. Becker, J. E. Wittig and R. A. Zuhr, *Proc. Mat. Res. Soc.* **244**, to be published (1992).
7. W. P. Halperin, *Rev. Mod. Phys.* **58**, 533 (1986).
8. R.H. Magruder,III, R.A. Zuhr and R.A. Weeks, *Nucl. Instrum. Meth. in Phys. Research B* **59/60**, 1308 (1991)
9. P. D. Townsend, *Rep. Prog. Phys.* **50**, 501(1987).
10. K. Becker, L. Yang, R. F. Haglund, Jr., R. H. Magruder, R. A. Weeks and R. A. Zuhr, *Nucl. Instrum. Meth. in Phys. Research B* **59/60**, 1304 (1991). Detailed descriptions of the Z-scan technique have been given by M. Sheik-Bahae, A. A. Said, T. Wei, D. J. Hagan and E. W. VanStryland, *IEEE J. Quant. Electron.* **26**, 760 (1990).
11. L. Yang, K. Becker and R. F. Haglund, Jr., to be submitted to *J. Opt. Soc. Am. B*.
12. L. Yang, K. Becker, and R. F. Haglund, Jr., *Bull. Am. Phys. Soc.* **35**, 1530 (1990).
13. G. L. Eesley, *Phys. Rev. B* **33**, 2144 (1986).
14. G. I. Stegemann and R. H. Stolen, *J. Opt. Soc. B* **6**, 652 (1989).

FIGURE CAPTIONS

Figure 1. Bright-field TEM image of metallic Cu nanoclusters formed by ion implantation in fused silica. The sample was implanted to a dose of $1.2 \cdot 10^{17}$ ions \cdot cm $^{-2}$. **Insert:** Electron diffraction image of the ring pattern characteristic of face-centered cubic copper in the ion-implanted layer.

Figure 2. Measured values of $\chi^{(3)}$ for the sample shown in Figure (1a), superimposed on a section of the absorption spectrum for the sample, shown in units of extinction coefficient per ion.

FIGURE CAPTIONS

Figure 1. Bright-field TEM image of metallic Cu nanoclusters formed by ion implantation in fused silica. The sample was implanted to a dose of $1.2 \cdot 10^{17}$ ions \cdot cm $^{-2}$. **Insert:** Electron diffraction image of the ring pattern characteristic of face-centered cubic copper in the ion-implanted layer.

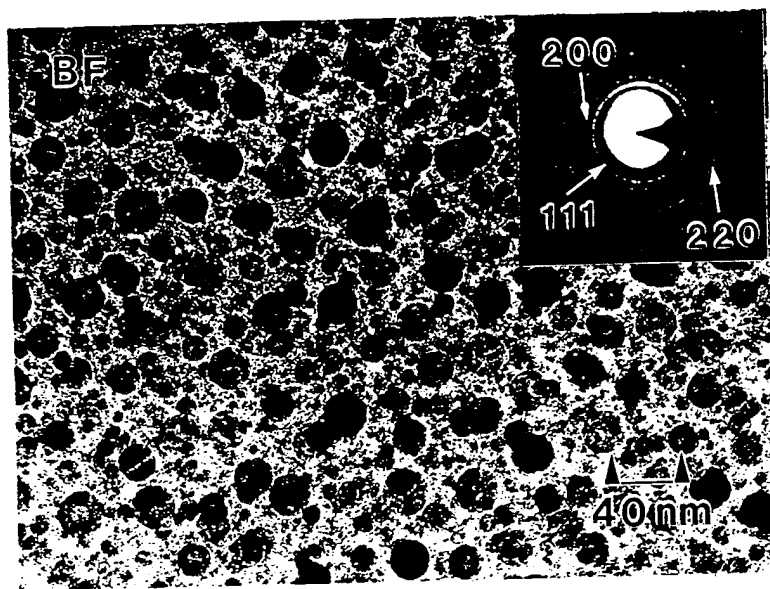


Figure 2. Measured values of $c^{(3)}$ for the sample shown in Figure (1a), superimposed on a section of the absorption spectrum for the sample, shown in units of extinction coefficient per ion.

